

Cycling comfort on asphalt pavement: Influence of the pavement-tyre interface on vibration



Jie Gao ^{a, e, **}, Aimin Sha ^{a, b, c, *}, Yue Huang ^d, Zhuangzhuang Liu ^{a, b}, Liqun Hu ^{a, b}, Wei Jiang ^{a, b}, Di Yun ^a, Zheng Tong ^f, Zhenjun Wang ^{b, c}

^a School of Highway, Chang'an University, Xi'an, 710064, China

^b Engineering Research Central of Pavement Materials, Ministry of Education of PR China, Chang'an University, Xi'an, 710061, PR China

^c School of Materials Science and Engineering, Chang'an University, Xi'an, 710061, China

^d Institute for Transport Studies, University of Leeds, Leeds, LS2 9JT, United Kingdom

^e Department of Civil Engineering, Liverpool John Moores University, Peter Jost Enterprise Centre, Byrom Street, L3 3AF, Liverpool, United Kingdom

^f Sciences et Technologies de Information et des Systèmes, Université de Technologie de Compiègne, Compiègne, 60319, France

ARTICLE INFO

Article history:

Received 16 July 2018

Received in revised form

11 March 2019

Accepted 12 March 2019

Available online 17 March 2019

Keywords:

Cycling comfort

Vibration

Asphalt pavement

Pavement-tyre interface

Pressure film

3D scanning and 3D printing

ABSTRACT:

Attainment of cycling comfort on urban roads encourages travelers to use bicycles more often, which has social and environment benefits such as to reduce congestion, air pollution and carbon emissions. Cycling vibration is responsible for the cyclists' perception of (dis)comfort. How asphalt pavement's surface characteristics relate to cycling comfort, however, remains undiscovered. In this study, the cycling vibration intensity on 46 sections of 24 urban roads was tested using a dynamic cycling comfort measure system while the cyclists' perception of vibration was identified via questionnaires; the cycling comfort was then defined based on the cycling vibration. To record the accurate pavement-tyre interface under a stable environment, a total of 19 pavement sections were scanned using a 3D digital camera. These 3D models were then 3D printed, which are used to conduct the pressure film test using a self-developed pavement-tyre interface test system. Three ranges of pressure films were adopted to characterize the pavement-tyre interface via 9 parameters, namely contact area (A_c), unit bearing area (B_u), stress intensity (S_i), stress uniformity (S_u), kurtosis (S_{ku}), spacing (Sp_a), maximum peak spacing (Sp_{max}), radius ratio (R_r) and fractal dimension (F_d), in consideration of the area characteristics, pressure amplitude, peak spacing and shape of the interface. Finally, the significant interface parameters were identified, and the regression model between interface parameters and cycling comfort was established. Results show that the cycling vibration was described to be 'very comfortable' when the human exposure to vibration level (a_{vv}) was less than 1.78 m/s^2 ; 'comfortable' when the a_{vv} was between 1.78 m/s^2 and 2.20 m/s^2 ; and 'uncomfortable' when the a_{vv} was greater than 2.20 m/s^2 . The average stress on rear wheel-pavement interface is higher than that of the front wheel. $B_{u-0.6}$, $Sp_{a-0.6}$ and $F_{d-0.6}$ are significant to cycling vibration. The 2LW pressure film is recommended for use to measure the bicycle pavement-tyre interface. The recommended interface characteristics are less than 7 mm^2 of the unit bearing area, 6 mm of average spacing and 2.38 of fractal dimension. Finally, dense asphalt mixture performs better in providing cycling comfort than the gap-graded asphalt mixture. Results of this study contribute to current knowledge on bike lane comfort and pavement design, the findings should be interested in cyclists, transport planners, and road authorities.

© 2019 Elsevier Ltd. All rights reserved.

1. Introduction

* Corresponding author. School of Highway, Chang'an University, Xi'an, 710064, China.

** Corresponding author. Engineering Research Central of Pavement Materials, Ministry of Education of PR China, Chang'an University, Xi'an, 710061, PR China.

E-mail addresses: highway-gaojie@st.chd.edu.cn (J. Gao), ams@chd.edu.cn (A. Sha).

In the past few decades, automobile-oriented transport planning and policies have led to a dramatic increase in the number of vehicles, resulting in traffic congestion, air pollution, fossil fuel consumption and road traffic accidents. Recently, the non-motorized transport is gaining recognition of their

environmental, economic and social benefits from governments and the public worldwide, especially in developed countries. Cycling, in particular, is becoming a popular means of transport because of being enjoyable, environmentally-friendly and cost-effective (Zhang et al., 2015). Shared bicycle schemes are gaining great attention. Globally, more than 800 cities have started the bicycle sharing schemes (Ricci, 2015). In China, only a few thousands shared bicycles were operated using public fund in major cities before 2015. However, traffic congestion and air pollution in megacities such as Beijing and Shanghai have demanded a smarter and greener mode of transport, creating a booming market for shared bikes and attracted numerous private investments. Since 2015, various types and brands of shared bicycles have been increasingly seen on Chinese streets, including small and medium-sized cities. At present, there are 77 companies in the Chinese market offering 23 million shared bicycles to more than 400 million registered users, 17 billion trips have been made using shared bicycles (Luo, 2018). Apparently, cycling in China is not only an alternative mode of transport to motorized vehicles that citizens occasionally use, but also a healthy and desirable lifestyle. Consequently, the service quality of urban bicycle lanes has become increasingly important not only for safety reasons but also for cycling comfort.

Human comfort is a complex perception which is jointly influenced by the tactile, visual, auditory, olfactory and hygienic factors (Boduch and Fincher, 2009). The service level of cycling infrastructure was widely acknowledged by previous studies as the main factor affecting cycling comfort. For example, Calvey et al. (2015) conducted a questionnaire investigation to determine the significant factors from 24 indicators concerning the cycling environment, which are believed to have an influence on cycling comfort. It reported that the bike lane pavement type directly impacts the comfort rating of cyclists. Furthermore, the quality of bike lane surface is reported to be a key factor for cyclists to plan their routes (Rybarczyk and Wu, 2010).

How pavement quality influences the cycling comfort? It is proved in previous study that the cycling vibration intensity is responsible for cyclists' comfort (Gao et al., 2018), but the essential question is: What qualities of the pavement determine the cycling vibration? Pavement macro-texture, a road surface characteristic with wavelengths from 0.5 mm to 50 mm, is reported to be crucial to cycling vibration (Chou et al., 2015). For instance, Hözel et al. (2012) compared the cycling vibration on asphalt pavement, concrete slabs, bound gravel, and cobblestones. Results indicated that the asphalt pavement provides much better cycling comfort compared with others. Importantly, Li's group (Li et al., 2013a, 2013b) first introduced the asphalt pavement macro-texture in terms of mean profile depth (MPD) to the investigation of cycling quality. Results showed that the MPD is significant with the cycling vibration, and the prediction model they developed has significant practical values. However, the mechanism of how the pavement macro-texture affects the cycling comfort is still unknown, partly because the MPD alone is insufficient to evaluate pavement macro-texture as it can only characterize the macro-texture in height. Apparently, there is a knowledge gap between cycling vibration and pavement macro-texture, which needs to be filled by an effective research approach and field data. The interface between the bicycle tyre and pavement surface reflects the actual contact area and distribution of stress. Therefore, the pavement-tyre interface can be considered as a key connection between cycling vibration and macro-texture. However, there is very little such research seen in previous publications.

In addition, previous studies have developed several cycling vibration evaluation methods, which were mainly based on field test which captured vibration signals by installing accelerometers

on the probe bicycle. However, it is a time-consumption task to ride a bicycle on the network periodically to evaluate the cycling quality, considering the massive road network. Therefore, transport planners and road authorities need a method with higher efficiency and accuracy.

In summary, the following questions should be answered when addressing aforementioned issues faced by transportation professionals.

- How does the pavement-tyre contact interface influence the cycling vibration?
- Which characteristics can be used to best determine whether an existing pavement is comfortable for cycling?

In this study, the cycling vibration intensity on 46 sections of 24 urban roads was tested via a dynamic cycling comfort measure system while the cyclists' perception of vibration was identified via questionnaires, then the cycling comfort was defined based on the cycling vibration. A total of 19 pavement sections were 3D digital scanned and then 3D printed in order to conduct the pressure film test under a stable environment, thereby a more precise theoretical study can be implemented. Therefore, laboratory test is recommended by previous studies (Chen et al., 2017; Zhang et al., 2014). In addition, the 3D printed model comes to the feasible option for the pressure film test as we are not allowed to cut off the urban pavement for laboratory test. In summary, three types of pressure film with different measurable ranges were adopted to quantitatively characterize the pavement-tyre interface using 9 parameters, which are contact area (A_c), unit bearing area (B_u), stress intensity (S_i), stress uniformity (S_u), stress kurtosis (S_{ku}), average stress peak spacing (Sp_a), maximum stress peak spacing (Sp_{max}), radius ratio (R_r) and fractal dimension of contact pattern (F_d). In addition, the correlation between interface parameters and cycling comfort was established. Finally, the interface characteristics for a comfortable bike lane are recommended and the cycling comfort detection method is suggested. The test method, analysis and evaluation procedure are illustrated in Fig. 1.

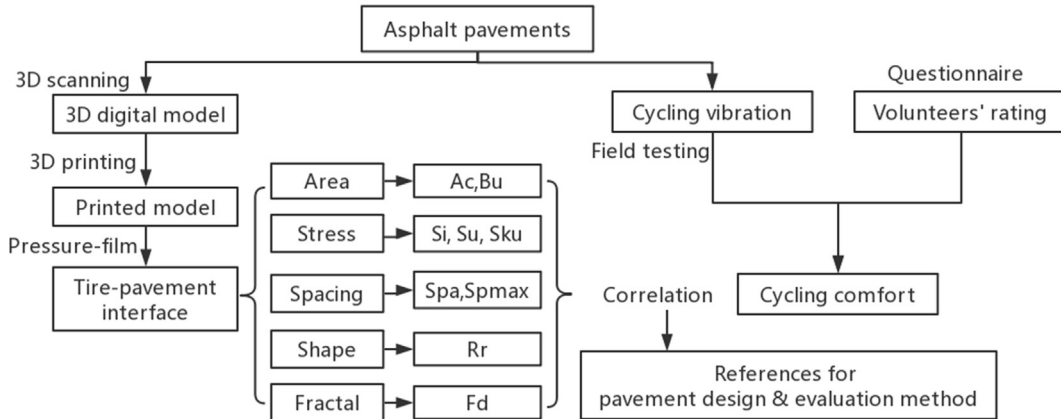
This study was carried out at a time when the Chinese government set bicycle transport as a strategy for sustainable urban development. Currently, there are no specific standards or guidance for cycle lane pavement materials design and cycling quality evaluation. Outcomes of this study will help road contractors to build high-comfort bike lane, for transport planners and road authorities to monitor cycling lane quality, and for government to encourage people to use shared bicycles, therefore, improving the urban transport environment.

2. Experiments

2.1. Measurement of cycling comfort

2.1.1. Tested road sections

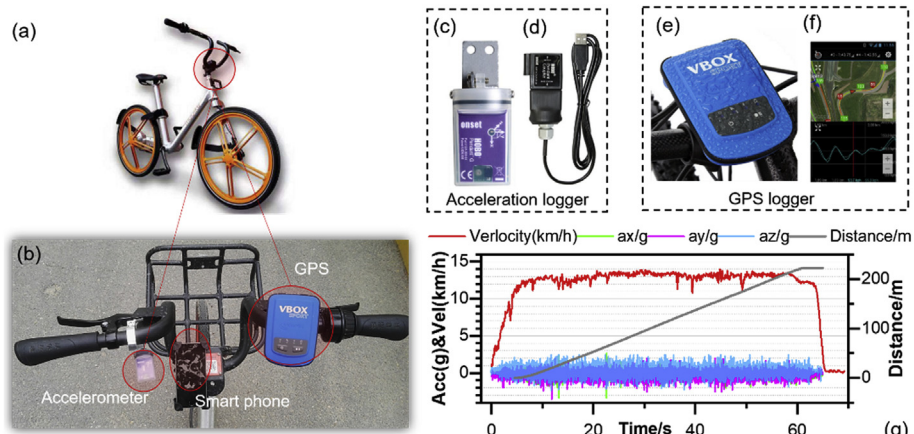
Cycling vibration on the 46 sections of 24 urban asphalt roads (11,500 m in length) was tested, as shown in Fig. 2. Furthermore, 19 out of the 46 road sections were selected to study the pavement-tyre interface, because these 19 road sections share a similar roughness (1.5 mm–1.8 mm) measured by using 3-m-straightedge method, which is recommended in a Chinese specification (JTGF40-2004, 2004), thereby the potential influence of pavement unevenness on the cycling vibration can be avoided. In addition, the selected sections all have high-quality asphalt pavement, located in the non-motorized lanes with low traffic volume and with no severe cracks or potholes. Previous surveys show that these road sections have the gradient of 0.5%–1.5% and horizontal curve radius is between 600 m and 1200 m.

**Fig. 1.** Test method, analysis and evaluation procedure.**Fig. 2.** Tested pavement sections in Xi'an city, China.

2.1.2. Cycling vibration test

A self-developed Dynamic Cycling Comfort (DCC) measure system was designed to record the cycling profiles, as shown in Fig. 3 (b). The bicycle (25 kg, using inflatable tyre) for the experiment was a shared bicycle (see Fig. 3 (a)) which is a common one seen in Chinese cities. Moreover, a skilled cyclist was recruited from a local cycling club to conduct the vibration test, who is a 28-years old

healthy male (weight 83 kg, height 177 cm) with over 6000 km of cycling experience. An acceleration data logger (HOBO Pendant G, made in USA), as shown in Fig. 3 (c), was firmly installed on the left handlebar of the bicycle, its technical parameters are measurement range $\pm 29.4 \text{ m/s}^2$, accuracy 0.735 m/s^2 , resolution 0.245 m/s^2 . The sampling rate was 100 Hz. Please note that the DCC system was designed to collect the vibration signal on the hand-bar instead of

**Fig. 3.** Dynamic Cycling Comfort (DCC) Measure System.

(a) shared bicycle for testing; (b) DCC installation; (c) acceleration logger; (d) controller and connector of acceleration logger; (e) VBOX sport GPS logger; (f) user interface of GPS app shown on a smartphone; (g) a typical cycling profile.

saddle and peals to represent the overall vibration that a cyclist perceived, and the vibration - cyclists' comfort relationship was pre-defined by conducting the questionnaire survey. If for the whole-body cycling vibration measurement only, the DCC may not suitable considering the lower sampling rate and difference in the measurement location, therefore, it is suggested to strictly follow the instruction given in standards (Griffin, 1990; ISO-2631, 1997; Taylor et al., 2017). For example, Taylor et al. (2018) have proposed a standard procedure and equipment for measuring cycling vibration. A VBOX sport data logger was installed on the right handlebar, as shown in Fig. 3 (b). The GPS records time (accuracy 0.1 s), position (2D position: $\pm 5 \text{ m}^*$) and velocity (accuracy 0.1 km/h) etc. Meanwhile, a VBOX app was installed on a smartphone (as shown in Fig. 3 (f)) to monitor the cyclist's real-time state.

Cyclist begins cycling along the assigned route with a constant speed (12–16 km/h). During the test, the cyclist refrains from shaking the bicycle handlebar, especially in the vertical direction. Cycling test would be re-conducted if any anomalies were found in the test data. Each section was tested three times to reduce random error. The average sampling length for each test section was around 250 m, the duration of each test exceeded 60 s. A typical cycling profile that the DCC recorded is illustrated in Fig. 3 (g).

The calculation of cycling vibration (a_{wv}) was undertaken by using international standard ISO 2631 (ISO-2631, 1997), using the vibration signals on x (a_{wx}), y (a_{wy}), and z (a_{wz}) axis for the duration of the measurement T . The used frequency weighting curve was W_k . The a_{wx} , a_{wy} , and a_{wz} can be calculated from Eq. (1) while the whole-body vibration level a_{wv} was obtained from Eq. (2).

$$a_{wi} = \left[\frac{1}{T} \int_0^T a_{wi}^2(t) dt \right]^{1/2}; i = x, y, z \quad (1)$$

$$a_{wv} = \sqrt{a_{wx}^2 + a_{wy}^2 + a_{wz}^2} \quad (2)$$

2.1.3. Cyclist' perception of vibration

Comfort is a subjective experience depending on individuals' perception. Therefore, a total of 17 volunteers were recruited to complete the questionnaire, and their assessments of vibration (and comfort) after cycling on each selected pavement section were recorded. Details of the questionnaire, volunteers and test procedures are described in our another publication (Gao et al., 2018). The key findings are summarised in section 3.1 of this paper.

2.2. 3D laser scanning of asphalt pavements

A 3D scanner (HandySCAN 300 produced by CREAFORM Inc, Canada) was adopted to sample the 3D digital information of the tested pavement surfaces. Technical specifications of the scanner were 0.100 mm resolution, 0.040 mm precision, and 205,000 measurements/sec sampling rate. Coordinates of the test area can be obtained with the assistance of position marks. Therefore, a self-made sampling frame with randomly affixed position marks was developed, whose effective sampling area was 9 cm \times 50 cm, as shown in Fig. 4 (a). 3D scanning involves four steps: i) follow the GPS navigation to find the road sections where the vibration test was conducted; ii) select the representative areas with no significant surface difference (visual inspection) on the bicycle lane recorded by the GPS, and use a sampling frame to limit the scan area; iii) brush off debris from the selected area before the measurement starts, as shown in Fig. 4(a); iv) scan the selected areas, as shown in Fig. 4(b). Three area with no significant difference was scanned to represent a road section.

The 3D models should be firstly trimmed to have the same dimensions since the original models covered unnecessary area, then eliminate the lateral and longitudinal difference caused by road slopes using the least-squares-fitting. The typical reconstructed 3D models for each section are shown in Appendix A.

2.3. 3D printing of scanned model

A fused deposition modeling (FDM) 3D printer (CR-10 produced by Creality 3D Technology Co., Ltd, China) was used to create the 3D models of pavement surfaces using polylactic acid material (PLA). The critical technical specifications of the 3D printer are ± 0.1 mm print accuracy and 0.4 mm nozzle diameter. The main properties of the used PLA materials are $1.25 \pm 0.05 \text{ g/cm}^3$ density, $\geq 60 \text{ MPa}$ tensile strength and $\geq 60 \text{ MPa}$ bending modulus. PLA has the desirable mechanical properties under bending and tensile loading, and shows no significant deformation under the applied load (Song et al., 2017), therefore, the distribution of stress over the pavement-tire remained unchanged during the loading.

Three steps were involved in the 3D printing process. i) Materialization of the surface model. The original 3D scan model is a surface model which cannot be printed because it is not an entity with volume and centroid. Therefore, boundaries of the original surface model are stretched down to the same height by computer animation, and then the new boundary is sealed to form a printable entity. ii) Model optimization. Original surface models often have defects such as self-intersection, high folding edges, and missing information, thus the original models should be examined and repaired using a commercial software. iii) Model support during

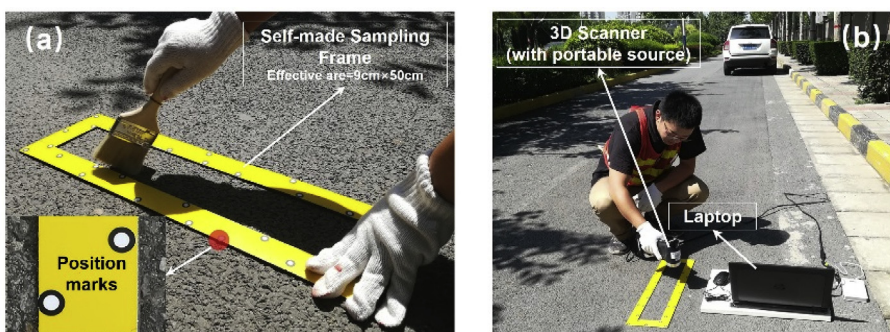


Fig. 4. Field 3D scanning for the pavement surfaces.
(a) sampling frame with position marks; (b) 3D scanning.

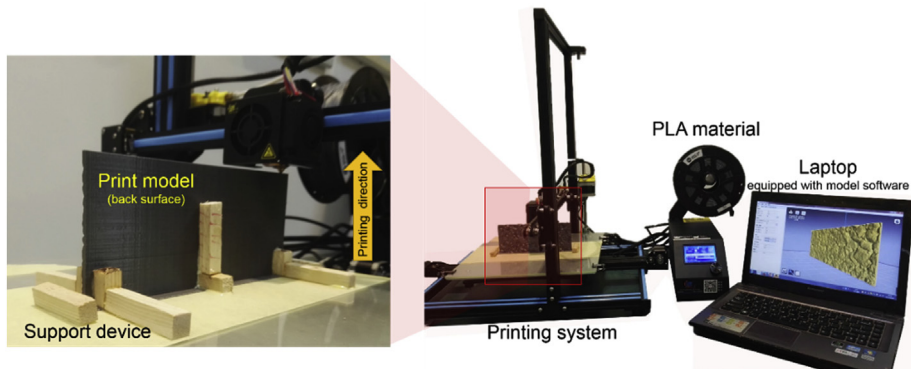


Fig. 5. 3D printing.

printing. It is necessary to use support device to keep the model stable, which is the wood sticks in this study, as shown in Fig. 5.

Five technical settings are recommended to obtain a high-quality printing model (Creality 3D Technology Co., 2017). After several adjustments of printing parameters, the optimal printing settings for use were 0.8 mm wall thickness, 0.1 mm layer thickness, 100% triangle sampling rate, 100% filling rate and 200 °C nozzle temperature. Three representative areas were randomly selected from three 3D surfaces and were printed for each road section. The dimension was 8 cm × 20 cm × h, in which the height (h) of the printed model is at least 5 mm higher than the maximum texture depth. Some printed models were shown in Fig. 6.

2.4. Pressure-sensitive film test

2.4.1. Pressure film

The two-sheet type pressure film is composed of two PET base material films which are coated with the color-forming layer (upper) and color-developing layer (lower). The microcapsules inserted in the color-forming layer are broken under the applied pressure; then the colorless pigments are released from micro-capsules and absorbed by the developer, producing a red color because of chemical reaction. The microcapsules containing the color-forming materials are adjusted to varying sizes and strengths,

producing a color density that corresponds to the amount of pressure. Once the temperatures and humidity of testing environment are determined, the pressure on the film can be converted in proportion to its color density (Fujifilm, 2015).

Three types (4LW, 3LW, and 2LW) of pressure films were used. The measurement pressure ranges of 4LW, 3LW, and 2LW are 0.05–0.2 MPa, 0.2–0.6 MPa, 0.5–2.5 MPa, respectively. Pressure films are sensitive to test environment, the recommended test temperature ranges are 20–30 °C (35–80% humidity), 15–35 °C (35–80% humidity), and 20–35 °C (20–75% humidity) for 4LW, 3LW, and 2LW, respectively.

Pressure film allows the measurement of the tyre-pavement interface, and has a higher measuring point density compared with others, such as the pressure plate method, pressure sensitive membrane, and pressure sensors, etc. It has a single measurement point area of 0.016 mm², therefore, even the finest details can be detected (Cheli et al., 2011; Liang et al., 2013). Meanwhile, the contact pattern is difficult to be distorted because the ultra-thin film (0.1 mm) is easy to fits the pavement surface.

2.4.2. Test procedures

As previously discussed, the test environment has significant effect on pressure film test accuracy. To create a stable test environment, a purpose-designed test system was established, which

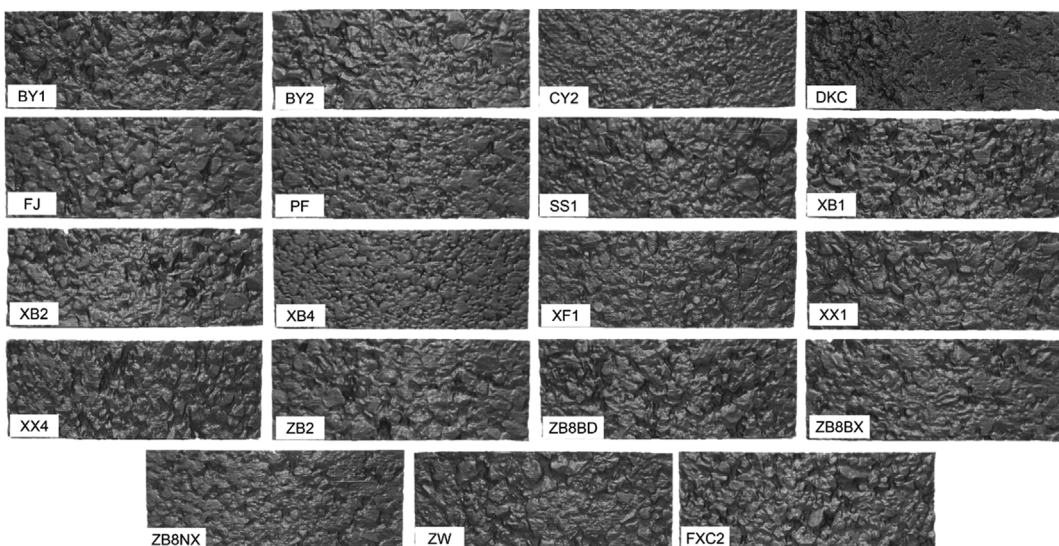


Fig. 6. Typical 3D printed model for each road section.

consists of two subsystems in consideration of the environment and stability factors, as shown in Fig. 7 (a). Environment subsystem consists of a temperature-controlled heating plate, a hygrometer and a thermal camera to monitor surface temperature. Stability system was designed to eliminate the interference of human behavior in test. It consists of a benchmark for monitoring transversal stability (see Fig. 7(b)), while a bracket, limit buckles and a bicycle brake were used to maintain longitudinal stability, as shown in Fig. 7(a, c).

Before the test, the heating plate, 3D printed model, and pressure film ($7 \text{ cm} \times 15 \text{ cm}$) were placed in sequence as shown in Fig. 7 (d). Then set the temperature at 30°C and heated them together for at least 10 min (depends on room temperature). When the temperature recorded in the thermal camera reached stable (30°C), record the humidity shown in the hygrometer. After adjustments made by the cyclist (the same person who participated in the vibration test), the tyre (see Fig. 7(e)) was pressed vertically on the film and was held for $2\text{min} \pm 5\text{sec}$ while the cyclist was seated on the test bicycle. During the test, any shakes or rotations on the bicycle were not allowed and the pressure film would be abandoned if such behaviors happened. A typical contact interface recorded on the pressure film is shown in Fig. 7 (f). Three films were obtained for each 3D model.

2.5. Parameters

Natural pattern, for example, the pavement-tyre interface, are complex and anomalous, which is difficult to be characterized via a few parameters and there is no ideal geometric model that can fully describe the relationships. The scope of the survey aimed to be as comprehensive as possible since the parameters that may potentially affect cycling vibration are not fully understood in current knowledge. Three ranges of pressure films were adopted to characterize the pavement-tyre interface using 9 parameters, namely contact area (A_c), unit bearing area (B_u), stress intensity (S_i), stress uniformity (S_u), kurtosis (S_{ku}), spacing (Sp_a), maximum peak spacing (Sp_{max}), radius ratio (R_r) and fractal dimension (F_d), in consideration of the area characteristics, pressure amplitude, peak spacing and shape of the interface. Each parameter is described as follows.

2.5.1. Stress

Average stress intensity (S_i , MPa) indicates the average stress level of pavement-tyre contact interface. Stress uniformity (S_u , MPa) describes the difference in stress across the interface, it can be calculated using Eq. (3), where, S_j is the stress value of the j th point.

$$S_u = \sqrt{\sum_{j=1}^n (S_j - \bar{S})^2 / n} \quad (3)$$

Kurtosis (S_{ku}) relates to the uniformity of the pressure amplitude distribution function (ADF) or, equivalently, to the sharpness of the pressure distribution. S_{ku} can be calculated by Eq. (4) (ISO4287, 1997).

$$S_{ku} = \frac{1}{AS_q^4} \sum_{i=1}^n Z^4(x, y) \quad (4)$$

Where A is the projection area; $Z(x, y)$ is the pressure values and (x, y) is used to identify the position of calculation point. S_q (root mean square pressure) is calculated by Eq. (5) as:

$$S_q = \sqrt{\frac{1}{A} \sum_A Z^2(x, y)} \quad (5)$$

2.5.2. Area

Two parameters may have a potential influence on cycling vibration. The first is contact area of the interface (A_c , mm^2). The second is the unit bearing area (B_u , cm^2), which equals to the contact area (A_c) divided by the number of the isolated grain-like objects in the interface pattern (n_{ob}), it is calculated via Eq. (6).

$$B_u = \frac{A_c}{n_{ob}} \quad (6)$$

2.5.3. Spacing

Average stress peak spacing (Sp_a) describes the distance between pressure peaks in the pressure profile along the traffic direction, it can be calculated using Eq. (7). The original pressure profiles were processed using a low-pass filter with the cut-off length of 1 mm to remove the fine peaks, which is resulting from the micro-texture of aggregates, a typical original profile and filtered profile is demonstrated in Fig. 8 (a). At least 5 profiles were extracted from an interface image with an equal interval for calculation of Sp_a , as shown in Fig. 8 (b). Furthermore, the average of the maximum stress peak spacing (Sp_{max}) of five profiles was identified.

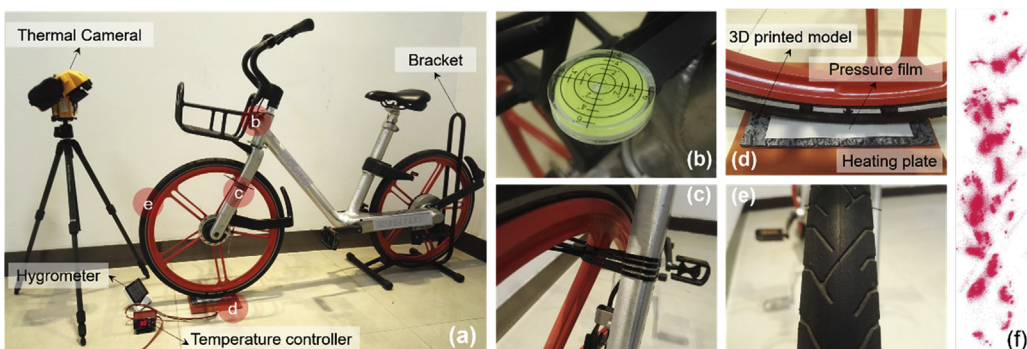


Fig. 7. Pressure film test system for pavement-bicycle tyre interface.

(a) overview of the test system; (b) benchmark; (c) limit buckle; (d) contact area; (e) tyre surface; (f) a typical contact interface recorded on the 2LW film.

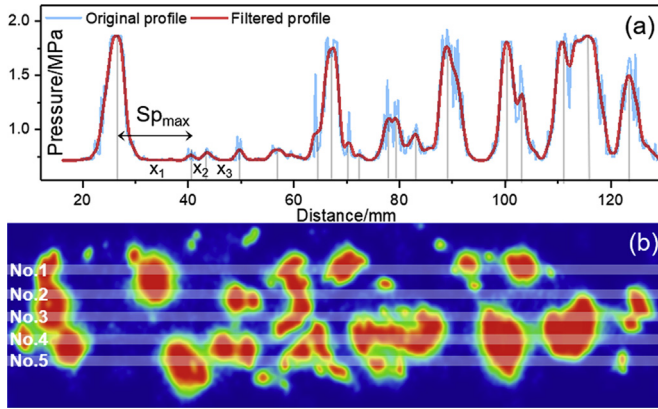


Fig. 8. Spacing calculation.

(a) original and filtered stress profile; (b) five profiles extracted in an equal interval.

$$Sp_a = \frac{\sum_{i=1}^n (x_{i+1} - x_i)}{n - 1} \quad (7)$$

Where, x_i is the coordinate of the i th pressure peak on a pressure profile, mm; n is the total number of peaks in a profile.

2.5.4. Shape

The average radius ratio of all grain-like objects R_r (no unit) describes the general geometric shape of the grain-like objects on the interface, it can be calculated with Eq. (8). Where l_{max} is the max radius of an object, l_{min} is the min radius of an object. The greater the R_r , the slender of the grain-like object is.

$$R_r = \frac{\sum_i^n l_{max}}{n_{ob}} (i = 1, 2, 3 \dots n) \quad (8)$$

2.5.5. Fractal dimension

Fractal dimension is widely accepted as an effective way of processing images for pattern analysis (Nayak et al., 2018). The original patterns were converted into grayscale images, then the power spectrum fractal dimension was used to evaluate the pattern appeared in the pressure films. Power spectrum method is based on the power spectrum dependence on fractional Brownian motion, in which every grayscale profile that forms the image is Fourier transformed and is power spectrum evaluated. The fractal dimension F_d can be calculated using the slope β of $\lg S(k) - \lg k$. The relation between power spectrum $S(k)$ and frequency k can be found in Eq. (9). The fractal dimension F_d is expressed in Eq. (10). The power spectral density of a $N_x \times N_y$ size image is obtained by a two-dimensional Fourier transformation, as shown in Eq. (11), where v, μ are the frequency variables. Then the image power spectrum can be obtained via Eq. (12) (Van Put et al., 1994).

$$S(k) \propto k^{-\beta} \quad (9)$$

$$F_d = 4 + \frac{\beta}{2} \quad (10)$$

$$F(\mu, v) = \frac{1}{N_x N_y} \sum_{x=0}^{N_x-1} \sum_{y=0}^{N_y-1} Z(x, y) \exp \left[-j2\pi \left(\frac{\mu x}{N_x} + \frac{v y}{N_y} \right) \right] \quad (11)$$

$$S(k) = |F(\mu, v)|^2 \quad (12)$$

3. Results and discussion

3.1. Cyclist's perception of vibration

Fig. 9 demonstrates the results of cycling vibration test and perception test. The columns in the bar chart represent the vibration levels of the 46 road sections in ascending order of the vibration (a_{vv}), in which the 19 sections highlighted in blue were 3D printed. Correlation between the cycling vibration and the comfort perception is shown in red, 11 road sections were rated by volunteers. Cyclists' comfort is rated from 1 (very uncomfortable) to 5 (very comfortable).

Clearly, the range of vibration (a_{vv}) value is between 1.031 m/s^2 (XB-4) and 3.193 m/s^2 (XX-1), indicating that the cycling comfort among these sections can be quite different. The comfort level decreases with the increase of a_{vv} . In addition, no road section has been classified as 'very uncomfortable' or 'very comfortable' although a few volunteers voted such for some sections. Therefore, there are three comfort levels were used in perception test, i.e. comfortable, intermediate and uncomfortable. According to the regression equation shown in Fig. 9, the comfort-vibration threshold can be defined as: i) the cycling was described as 'very comfortable' when the a_{vv} was less than 1.78 m/s^2 ; ii) 'comfortable' when the a_{vv} was between 1.78 m/s^2 and 2.20 m/s^2 ; and iii) 'uncomfortable' when the a_{vv} was greater than 2.20 m/s^2 . Based on the above cycling vibration-comfort threshold, 18 out (approximately 39%) of the 46 road sections are classified to be 'very comfortable' and 'uncomfortable' to cycle, respectively, and the rest 10 (approximately 22%) road sections are regarded as 'comfortable'. As such, the pavement-tyre interface characteristic can be linked to cycling comfort directly as the definition of cyclists comfort threshold in vibration is a quantified index (Gao et al., 2018).

3.2. Stress difference of pavement-tyre interface on front and rear wheel

Structural analysis of bicycles in previous studies has clearly indicated that the process of stress distribution among the components of a bicycle (Chou et al., 2015; Dao and Chen, 2012). However, the difference in stress distribution characteristics between the front and rear wheels of the bicycle have almost not seen in publications. To this end, the differences in stress distributions histogram and contact patterns of the pavement-tyre interfaces on the front and rear tyre are compared, the results are shown in Fig. 10. The first finding is that the average stress on rear wheel-pavement interface (1.705 MPa) is higher than that of the front wheel (1.182 MPa) according to 2LW pressure film. In contrast, the stress histogram of the rear and front wheels in both 3LW and 4LW peaked at the upper end of the measurement range, indicating that the applied stress has exceeded their measurable ranges. Therefore, there is only slight difference in average stress between the front (0.165 MPa in 4LW, 0.412 MPa in 3LW) and rear wheel (0.166 MPa in 4LW, 0.408 MPa in 3LW) presented in both 3LW and 4LW pressure film. Consequently, the 2LW pressure film is recommended for use in the pavement-tyre stress measurement.

In addition, the contact area on the rear wheel is greater than that of the front wheel. The contact area on the rear wheel in 2LW, 3LW and 4LW pressure film are 4.66 cm^2 , 6.155 cm^2 and 7.84 cm^2 , respectively, while on front wheel are 3.68 cm^2 , 5.26 cm^2 and 6.02 cm^2 , respectively. It is worth mentioning that although the

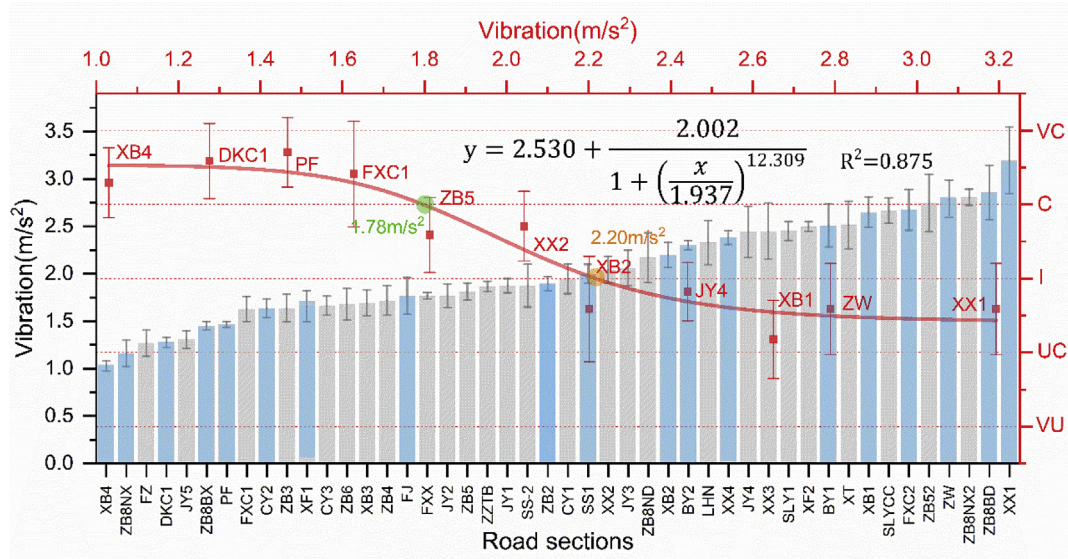


Fig. 9. Cycling vibration on the tested sections and the correlation between comfort perception and vibration.

Note: VC, C, I, UC and VU refer to the very comfortable, comfortable, intermediate, uncomfortable and very uncomfortable, respectively.

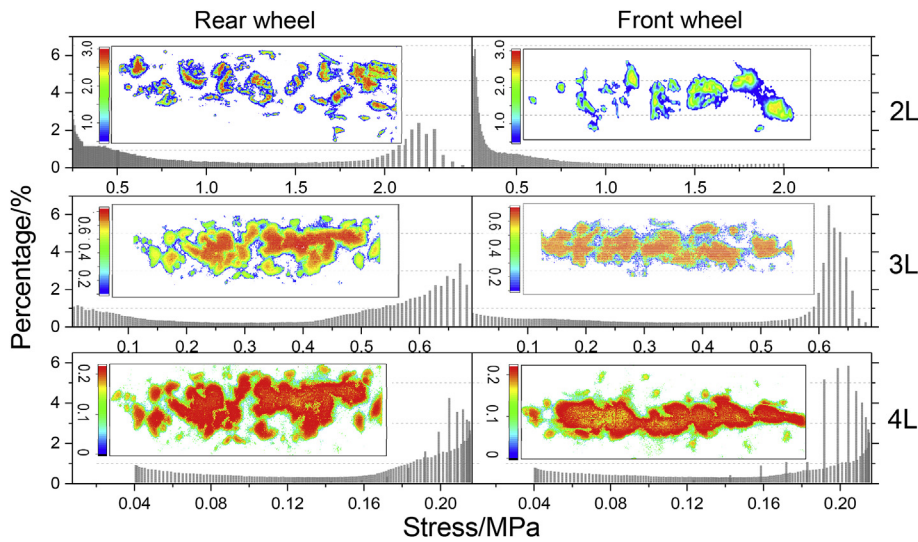


Fig. 10. Difference in stress on the rear and front wheel of the test bicycle (grey bars represent the stress histogram in percentage, %).

3LW and 4LW pressure film cannot accurately reflect the actual stress of the interface because of the limited stress measurement ranges. However, the 3LW and 4LW pressure film should not be excluded from the calculation of area parameters and shape features (see section 3.3) as they have not been proved ineffective in these aspects. After understanding the interface difference between rear and front wheel, the interface measurements in this work were based on the front wheel, where the accelerometer was installed to obtain the cycling vibration a_{vw} .

3.3. Effect of pavement-tyre interface characteristics on cycling vibration

Obtained pressure films of the pavement-tyre interfaces were converted into the stress distribution images, which are displayed in Appendix B. The following discussions are based on the calculations from these images. Five pressure ranges were divided using

three types of pressure films, as shown in Table 1. The parameters are explained as such: $A_{c-0.05}$ stands for the average contact area where stress was beyond 0.05 MPa; $S_{i-1,2}$ represents the average stress of the contact interface, where stress was less than 1.2 MPa was truncated.

3.3.1. Stress characteristics

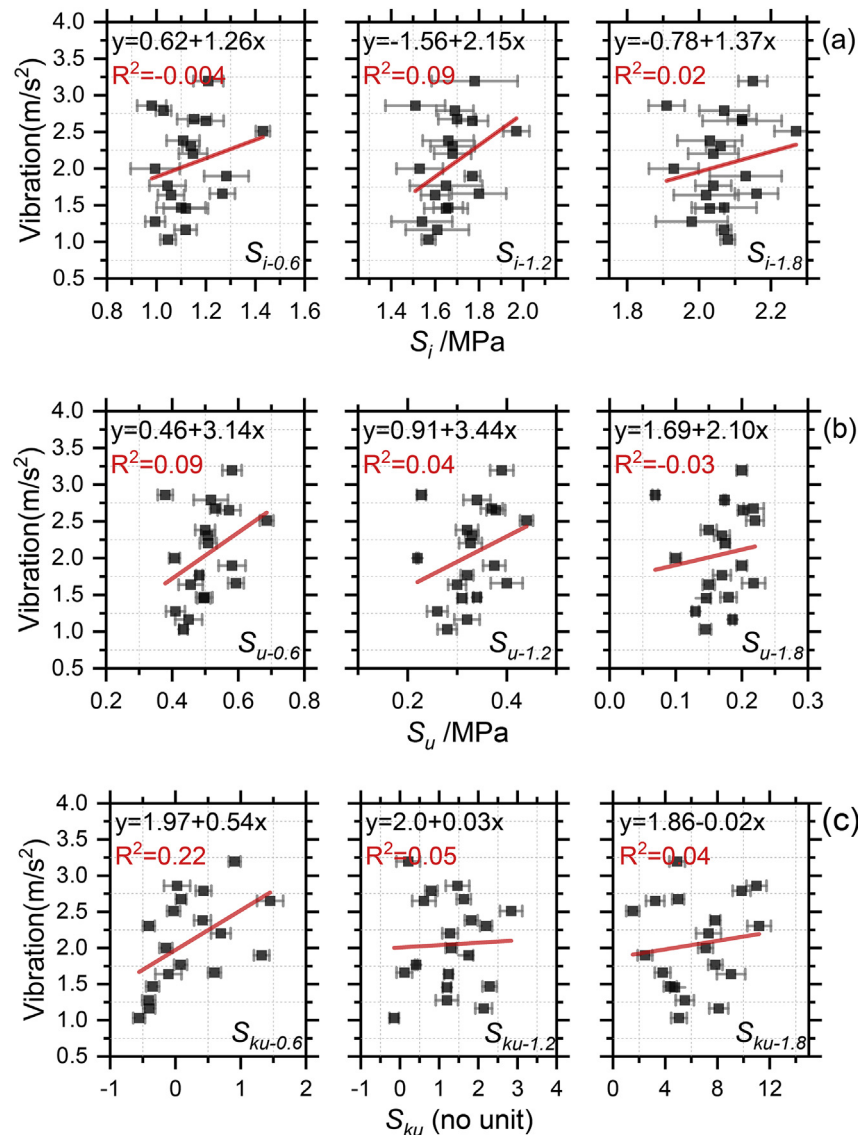
Section 3.2 has indicated that the stress measurement on 3LW and 4LW film was limited by their measurable ranges. Consequently, only stress recorded on the 2LW film is used for the calculation of stress characteristics. The stress characteristics are calculated based on three pressure levels (as shown in Table 1) divided from the 2LW film. The effect of the average stress intensity (S_i , MPa) and stress uniformity (S_u , MPa) on cycling vibration is illustrated in Fig. 11 (a) and (b). Obviously, no significant correlation between stress characteristics levels and cycling vibration can be found. It indicates that the intensity and uniformity of stress that acted on the

Table 1

Explanation of the parameters.

Film	Pressure ranges/MPa	Typical image	Parameters								
			Stress			Area		Spacing		Shape	
			S_i	S_u	S_{ku}	A_c	B_u	Sp_a	Sp_{max}	R_r	
4LW	[0.05, 0.2]		-	-	-	$A_{c-0.05}$	$B_{u-0.05}$	-	-	$R_{r-0.05}$	
3LW	(0.2, 0.6]		-	-	-	$A_{c-0.2}$	$B_{u-0.2}$	-	-	$R_{r-0.2}$	
2LW	(0.6, 2.5]		$S_{i-0.6}$	$S_{u-0.6}$	$S_{ku-0.6}$	$A_{c-0.6}$	$B_{u-0.6}$	$Sp_{a-0.6}$	$Sp_{max-0.6}$	$R_{r-0.6}$	$F_{d-0.6}$
	[1.2, 2.5]		$S_{i-1.2}$	$S_{u-1.2}$	$S_{ku-1.2}$	$A_{c-1.2}$	$B_{u-1.2}$				
	[1.8, 2.5]		$S_{i-1.8}$	$S_{u-1.8}$	$S_{ku-1.8}$	$A_{c-1.8}$	$B_{u-1.8}$				

Note: Typical images in Table 1 of 2LW, 3LW and 4LW are obtained from different positions in the same road section.

**Fig. 11.** Correlation between cycling vibration and S_i (a), S_u (b) and S_{ku} (c) presented on 2LW film and cycling vibration.

pavement-tyre interface has insignificant influence on cycling vibration, at least in the range of 0.6 MPa–2.5 MPa. This conclusion is similar with Torbic's study (Torbic et al., 2003), in which the mass of a bicyclist does not significantly affect cycling vibration when bicyclists mass in the range of 54–107 kg, namely the load applied on bicycle tyre-pavement interface does not change the intensity of

cycling vibration. On the other hand, it is estimated in previous studies that stress characteristics of the pavement-tyre interface have the direct influence on the skid resistance of road surface, which contributes to the riding safety (Li et al., 2018). This study simply justified that limited attention should be paid to stress characteristics when the cycling comfort is the main concern.

Generally, the stress histogram will present an ideal normal distribution when its kurtosis ($S_{ku-0.6}$) equal to 3. According to Fig. 11(c), the kurtosis of all tested samples is less than 3, which means the stress distribution curve on all interfaces are flatter than the normal distribution curve. In addition, the $S_{ku-1.2}$ and $S_{ku-1.8}$ increase more significantly compared to $S_{ku-0.6}$, indicating that higher stress ranges lead to a sharper stress distribution curve. However, no significant relationships can be concluded based on the relation between kurtosis and vibration, as shown in Fig. 11(c).

3.3.2. Area characteristics

The cycling vibrations on tested road sections are plotted against the unit bearing area (B_u) and contact area (A_c), respectively, as shown in Fig. 12 (a) and (b). Apparently, the $B_{u-0.05}$ (calculated from the interface on the 4LW film) and cycling vibration are statistically insignificant. On the contrary, the significant positive linear correlations between cycling vibration and $B_{u-0.2}$ as well as $B_{u-0.6}$ are demonstrated in Fig. 12 (a). Comparatively, $B_{u-0.6}$ has a higher correlation coefficient (0.71) with the vibration than that of $B_{u-0.2}$ (0.62). Therefore, the cycling vibration is more sensitive to the unit bearing area when the stress is 0.6 MPa–2.5 MPa. In the meantime, a weak correlation between $B_{u-1.2}$ and vibration can be observed and the $B_{u-1.8}$ presents no correlation. A pavement-tyre interface with lower unit bearing area is related to lower cycling vibration and higher cycling comfort.

Generally, the unit bearing area of the interface depends on the gradation of asphalt mixture and the angularity of the aggregates exposed on the road surface. Asphalt mixture with larger nominal aggregate size and higher proportion of coarse aggregates have higher unit bearing area. For example, as shown in Fig. 13 (a), the unit bearing area increases from AC-13 to AC-16 to SMA-20. This is because the area of single aggregate exposed on pavement surface increases with the size of the aggregate, this fact is supported by the stress pattern recorded on the pressure films. Furthermore, as shown in Fig. 13(b), coarse aggregate with ample angularity creates more contact points (grain-like objects) on the interface compared with smooth aggregates, therefore, the use of angular aggregates is beneficial to having higher unit bearing area and lower cycling vibration.

In Fig. 12 (b), the average contact area decreases significantly

with the increase of pressure ranges. The contact area shown in $A_{c-0.05}$ are within 550 mm²–900 mm² while this figure is 2 mm²–20 mm² under the stress level of 1.8 MPa–2.5 MPa. However, the correlation between A_c and cycling vibration in all stress ranges are very weak according to Fig. 12 (b). In summary, the unit bearing area of the pavement-tyre interface plays a more important role in cycling comfort than the contact area, indicating the stress distribution pattern matters more to the cycling vibration than the contact area.

3.3.3. Spacing characteristics

Average spacing (Sp_a) essentially reflects the distance between stress peaks along the travel direction. Therefore, the Sp_a was calculated by using the interface recorded on 2LW film as the stress peaks on the other two films are not observed due to limited measurable ranges, especially on the 4LW film. The $Sp_{a-0.6}$ and $Sp_{max-0.6}$ (as explained in Table 1) were adopted as spacing characteristics. In Fig. 14 (a), the average spacing between stress peaks of pavement-tyre interface is largely between 4 mm–7 mm. Furthermore, larger spacing of stress peaks results in higher cycling vibrations and lower cycling comfort. By this principle, the dense asphalt mixture would be preferred for use as surface materials for bike lanes to gap-graded asphalt mixture. In asphalt mixture, the gap between coarse aggregates is filled by finer aggregate. Generally, the degree of filling and thus level of compaction in dense asphalt mixture is much better than the gap-graded, as illustrated in Fig. 13 (a), in which the AC-13 and AC-16 are dense mixtures while the SMA-20 is a gap-graded mixture. Furthermore, the maximum distance between stress peaks is within 8 mm–23 mm, as shown in Fig. 14 (b). The correlation of the $Sp_{max-0.6}$ with cycling vibration is not as significant as $Sp_{a-0.6}$, indicating that the $Sp_{max-0.6}$ is a factor with limited influence on the cycling vibration.

3.3.4. Shape characteristics

The pavement-tyre interface is composed of the grain-like objects. The average radius ratio of all objects (R_r) is defined to represent the geometric shape of all the grain-like objects. In Fig. 15, the majority of the tested values is concentrated around $R_r = 5$ under all investigated stress levels, indicating that the grain-like objects on the interface present a narrow ellipse if assumed to

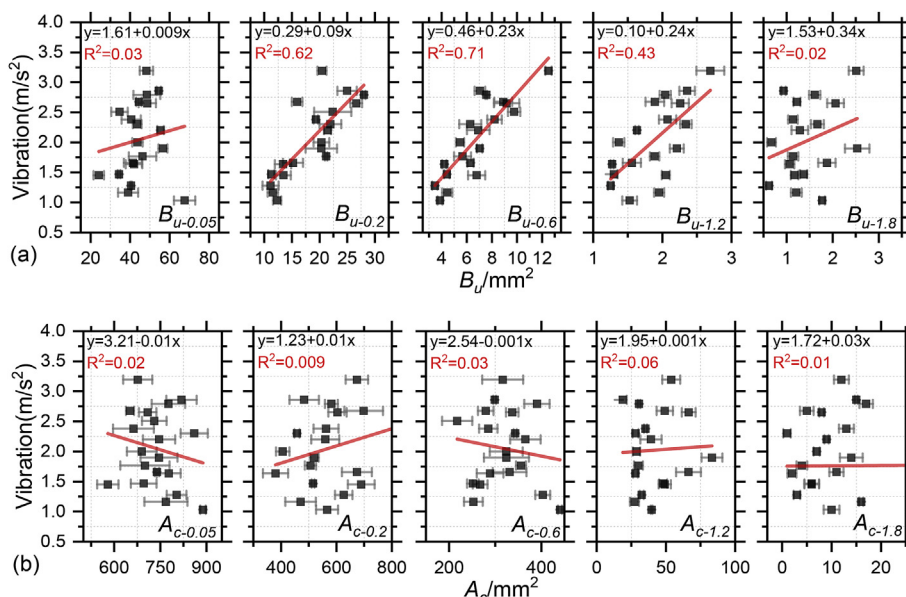


Fig. 12. Correlation between cycling vibration and B_u (a), A_c (b) and cycling vibration.

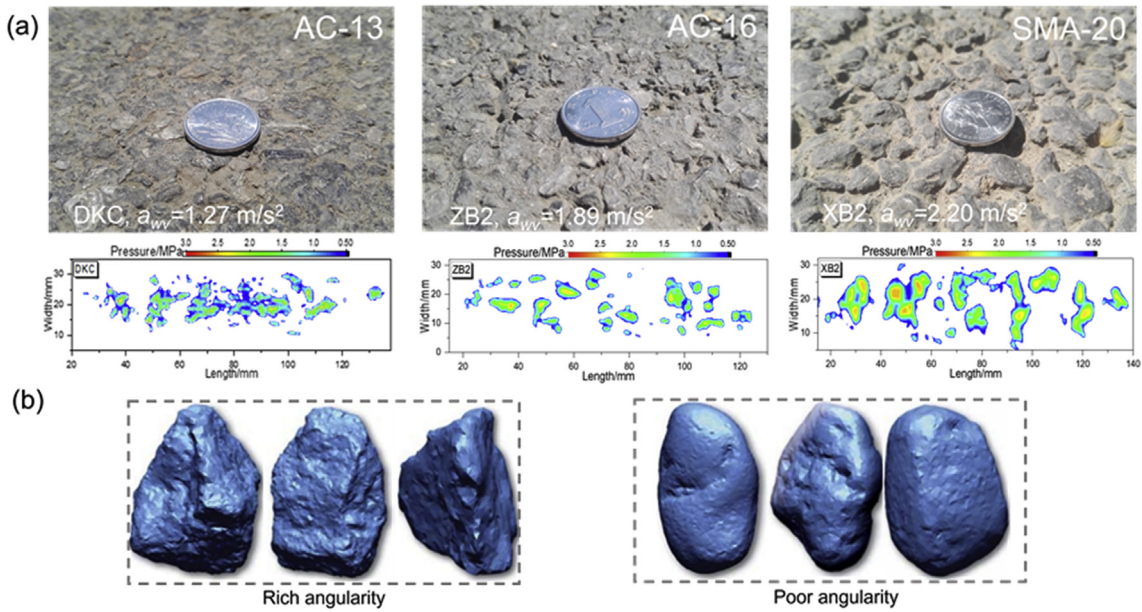


Fig. 13. Comparison on pavement surface and aggregate angularity.

Note: gradation type of the above road sections is obtained from local transport authority, but the gradation curves are not available. (a) picture of the tested pavement surfaces and stress distribution on the corresponding pavement-tyre interface on the 2LW film; (b) 3D scanning model of the coarse aggregates with good and poor angularity (Breytenbach et al., 2013).

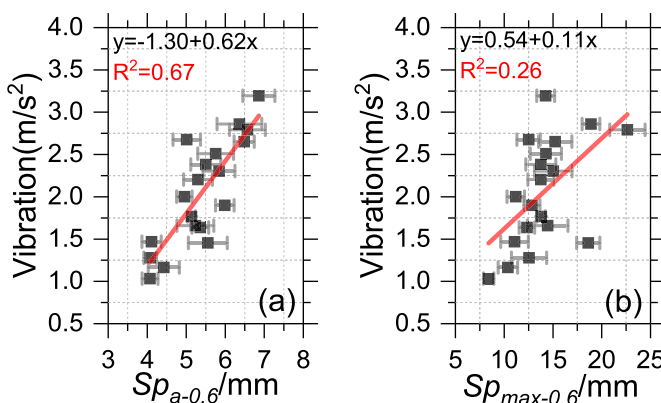


Fig. 14. Correlation between cycling vibration and $Sp_{a-0.6}$ (a), $Sp_{max-0.6}$ (b).

have an ideal geometric shape. However, no clear correlation can be observed between the R_r calculated from all types of pressure films and the cycling vibration. As a result, the shape of the grain-like

objects presented in the pressure film cannot be simplified to any known geometries as they are extremely irregular and complex.

3.3.5. Fractal dimension

Previous studies have reported that a rougher pavement surface has a higher fractal dimension (Hu et al., 2016; Zhang et al., 2017). The roughness of pavement surface, however, is a complex concept, which is potentially related with the space between aggregates and the shape of the aggregate itself. As shown in Fig. 16, the $F_{d-0.6}$ presents a significant linear correlation with the cycling vibration. The fractal dimension of the interface recorded on the 3LW and 4LW films was not involved in the calculation because the fractal dimension is magnitude-dependent and the limited stress on it can lead to erroneous results. The use of fractal dimension to characterize the stress pattern on interface is offering a novel measurement.

3.4. Practical recommendations

3.4.1. Recommendation for bike lane pavement design

After evaluating the correlation between cycling vibration and

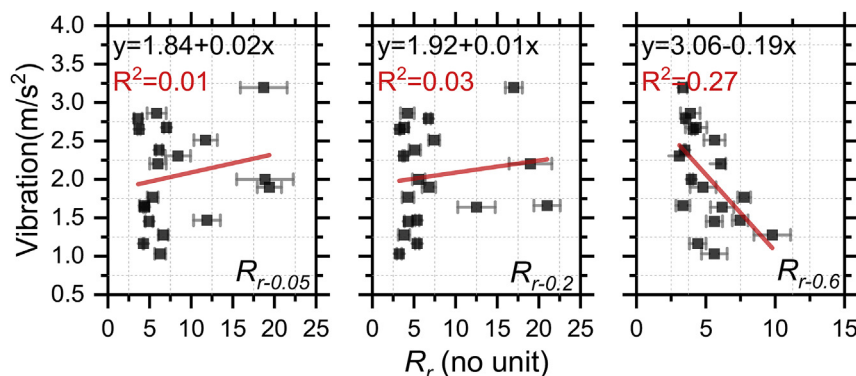


Fig. 15. Correlation between R_r and cycling vibration.

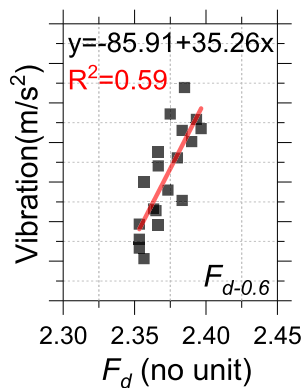


Fig. 16. Correlation between fractal dimension (F_d) and cycling vibration.

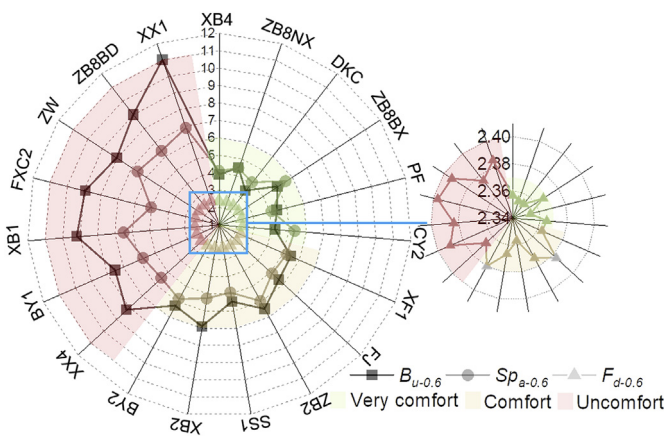


Fig. 17. Analysis on the commonality of road sections with the same classification of comfort.

the characteristics of the bicycle tyre-pavement interface concerning stress, area, spacing, shape and fractal dimension, five parameters ($B_{u-0.2}$, $B_{u-0.6}$, $B_{u-1.2}$, $Sp_{a-0.6}$ and $F_{d-0.6}$), are found to have correlation coefficient exceed 0.4, and thus are believed significant to cycling vibration. To recommend practical design of the interface characteristics, three parameters are selected which are $B_{u-0.6}$, $Sp_{a-0.6}$, and $F_{d-0.6}$. The reason is that $B_{u-0.6}$ has the higher correlation

coefficient with vibration compared to $B_{u-0.2}$ and $B_{u-0.2}$. In addition, the selected parameters are convenient for practical use because they are all obtained by using the 2LW pressure film.

Based on the results of cyclists' perception of vibration, to investigate the commonality of road sections with the same classification of comfort, three parameters are plotted in a radar diagram, as shown in Fig. 17. It can be seen that the road sections with the same classification of comfort have similar values of $B_{u-0.6}$, $Sp_{a-0.6}$, and $F_{d-0.6}$, indicating that the cycling vibration is influenced by these parameters synchronously rather than by a single parameter. After summarize the values range of $B_{u-0.6}$, $Sp_{a-0.6}$, and $F_{d-0.6}$ shown in Fig. 17, to design a cycling comfortable (including 'very comfortable') bike lane, the pavement material is recommended to have the following interface characteristics based on the 2LW pressure film: i) unit bearing area on 2LW below 7 mm²; ii) average spacing on 2LW below 6 mm; and iii) fractal dimension of the stress pattern on 2LW below 2.38.

3.4.2. Evaluation method of cycling comfort for bike lanes

Besides the recommendations for bike lane pavement design, it is useful to establish an evaluation method of cycling comfort for bike lanes in consideration the needs of road authorities and transport department to monitoring the cycling comfort on their properties. To this end, a multiple linear regression analysis of the interface and cycling comfort was carried out based on the interface obtained from the 2LW pressure film.

Three parameters ($B_{u-0.6}$, $Sp_{a-0.6}$ and $F_{d-0.6}$) are involved in this regression model. The statistical results are shown in Table 2. In Table 2, the Durbin-Watson is 1.865, indicating that the variables in this model do not present collinearity while the adjusted R^2 (0.953) indicates a desirable goodness of fit. Variance analysis shows the

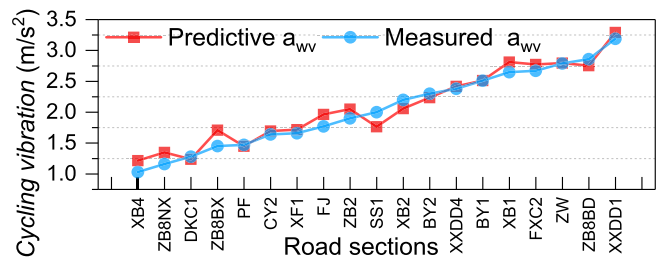


Fig. 18. Comparison between predicted and measured cycling vibrations.

Table 2
Statistical results.

Model	R	R^2	Model Summary		
			Adjusted R^2	Std. Error of the Estimate	Durbin-Watson
1	0.980 ^a	0.961	0.953	0.137	1.865
a. Predictors: (Constant), $B_{u-0.6}$, $Sp_{a-0.6}$, $F_{d-0.6}$					
b. Dependent Variable: Cycling vibration					
Sum of Squares		df	Variance analysis		
Regression		6.932	3	2.311	121.951
Residual		0.284	15	0.019	.000 ^b
Total		7.216	18		
			Coefficients		
			Unstandardized Coefficients		
			B	Std. Error	
(Constant)			-30.438	13.894	
$B_{u-0.6}$			0.140	0.037	3.782
$Sp_{a-0.6}$			0.262	0.122	2.146
$F_{d-0.6}$			12.704	6.026	2.108
			Standardized Coefficients		
			Beta		
			0.469		0.045
			0.313		0.002
			0.238		0.047
					0.048

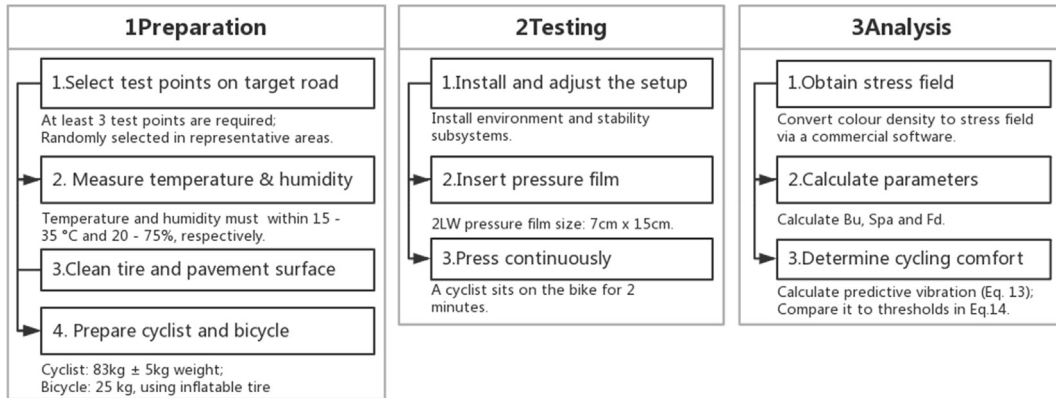


Fig. 19. Test procedure for on-site evaluation on cycling comfort of a pavement surface.

significance level is $\text{Sig} = 0.000 < 0.05$, indicating that the developed regression model is effective. Finally, the mathematical model between cycling vibration and pavement-tyre interface is given by Eq. (13). To verify the goodness of the developed regression model, a comparison is made between the measured vibration (ma_{wv}) and predicted vibration (pa_{wv}), the results are also shown in Fig. 18, in which only a slight difference is found. After obtained the pa_{wv} from Eq. (13), the cycling comfort can be determined by comparing the pa_{wv} with the perception results shown in Eq. (14).

In order to establish a solid and accuracy theory basis, this study particularly used the 3D printed model in the laboratory, however, it is acceptable to carry out the pavement-tyre interface test in the field if the test environment meets requirements of the pressure film. Based on our experiences, the test procedure for on-site evaluation on cycling comfort of a pavement surface is recommended, as shown in Fig. 19, in which the 3D scanning and 3D printing are not required, thus the evaluation method proposed herein has no barrier to practical uses. Meantime, the evaluation method is not limited to just used for field testing, but also for laboratory predicting on cycling comfort of prepared asphalt mixtures by replacing the pavement with an asphalt mixture slab.

Mathematical model

$$pa_{wv} = 0.140 \times B_{u-0.6} + 0.262 \times S_{pa-0.6} + 12.704 \times F_{d-0.6} - 30.438 \quad (13)$$

$$\text{Cycling comfort} = \begin{cases} \text{Very comfort; } pa_{wv} \in (0, 1.78) \\ \text{Comfort; } pa_{wv} \in [1.78, 2.20] \\ \text{Uncomfort; } pa_{wv} \in [2.20, 3.19] \end{cases} \quad (14)$$

4. Conclusions

The research has examined how pavement-tyre interface influences the cycling comfort in views from the pavement-tyre contact interface. It establishes a method for evaluating the cycling comfort, and provides recommendations for asphalt pavement design for bike lanes. The following conclusions can be drawn.

The cycling vibration was described to be ‘very comfortable’ when the a_{wv} was less than 1.78 m/s^2 ; ‘comfortable’ when the a_{wv}

was between 1.78 m/s^2 and 2.20 m/s^2 ; and ‘uncomfortable’ when the a_{wv} was greater than 2.20 m/s^2 .

The average stress and contact area on the rear wheel-pavement interface are greater than the front wheel. Basically, the cycling vibration is found to be related with the stress distribution in terms of unit bearing area ($B_{u-0.6}$), stress peaks spacing ($S_{pa-0.6}$) and fractal dimension ($F_{d-0.6}$), which are inversely proportional to the cycling comfort. On the contrary, no significant correlation can be found for the rest of parameters, namely the average stress intensity, kurtosis, contact area, average maximum peak spacing and average radius ratio.

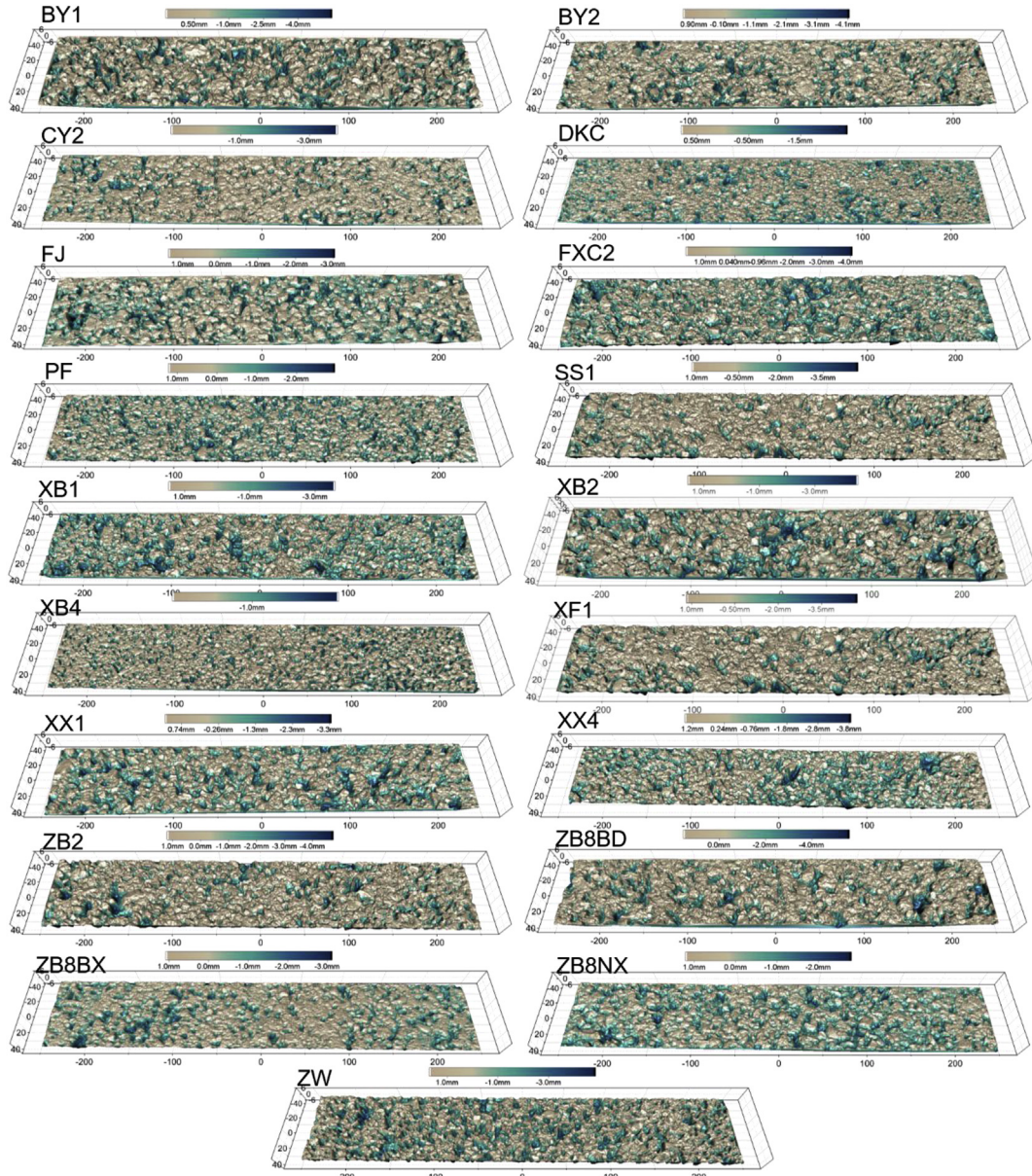
The 2LW pressure film is recommended for the measuring the bicycle pavement-tyre interface in preference to 3LW and 4LW. A bike lane pavement is believed to be comfortable for cycling if its pavement-tyre interface has the following attributes: less than 7 mm^2 of the unit bearing area, 6 mm of the average spacing and 2.38 of the fractal dimension. Generally, the dense-graded asphalt mixture performs better than the gap-graded mixture in cycling comfort.

Followings are our suggestions for the further studies. After understanding the correlation between pavement-tyre interface and cycling comfort, the specific cycling-friendly gradation of asphalt mixtures should be further studied and recommended through the comprehensive experiment. Nevertheless, the cycling comfort is only one aspect to be considered in the design and construction of bike lane; other factors, such as safety and durability, should not be compromised. Therefore, it is recommended in future study to establish a multi-criteria design and evaluation method that include skid resistance, pavement-tyre interface and fatigue resistance, etc.

Acknowledgment

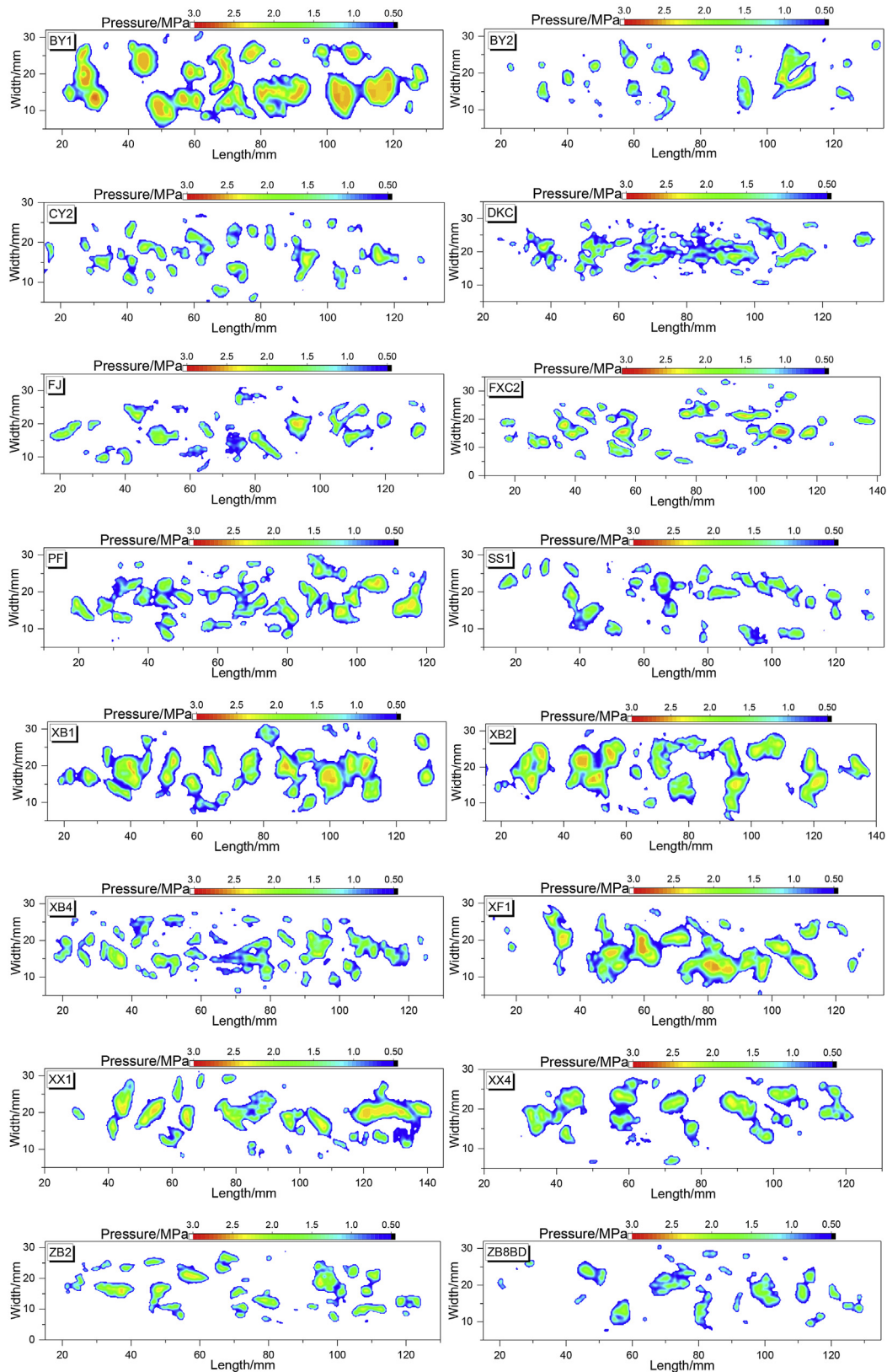
This work was supported by the China-UK Research and Innovation Partnership Fund (Newton Fund) jointly funded by China Scholarship Council and British Council, the National Key Research and Development Program of China (2018YFB1600200), the National Natural Science Foundation of China (Grant No. 51608043) and the Project of Key Laboratory for Special Region Highway Engineering of Ministry of Education (Grant No.300102218508). The authors greatly appreciate the valuable help offered by anonymous volunteers during our field and perception tests. Finally, the valuable assistance in 3D printing provided by Mr. Xiang Liu of Chang'an University is appreciated.

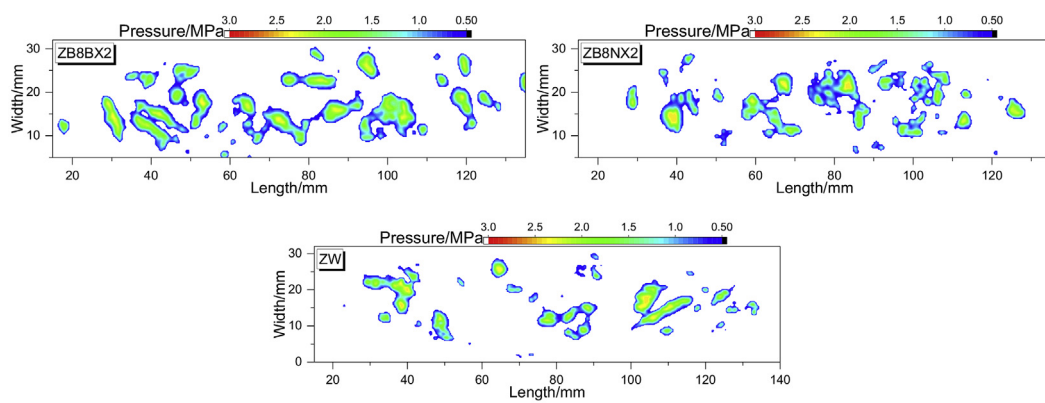
Appendix A. Typical 3D surfaces of the tested sections



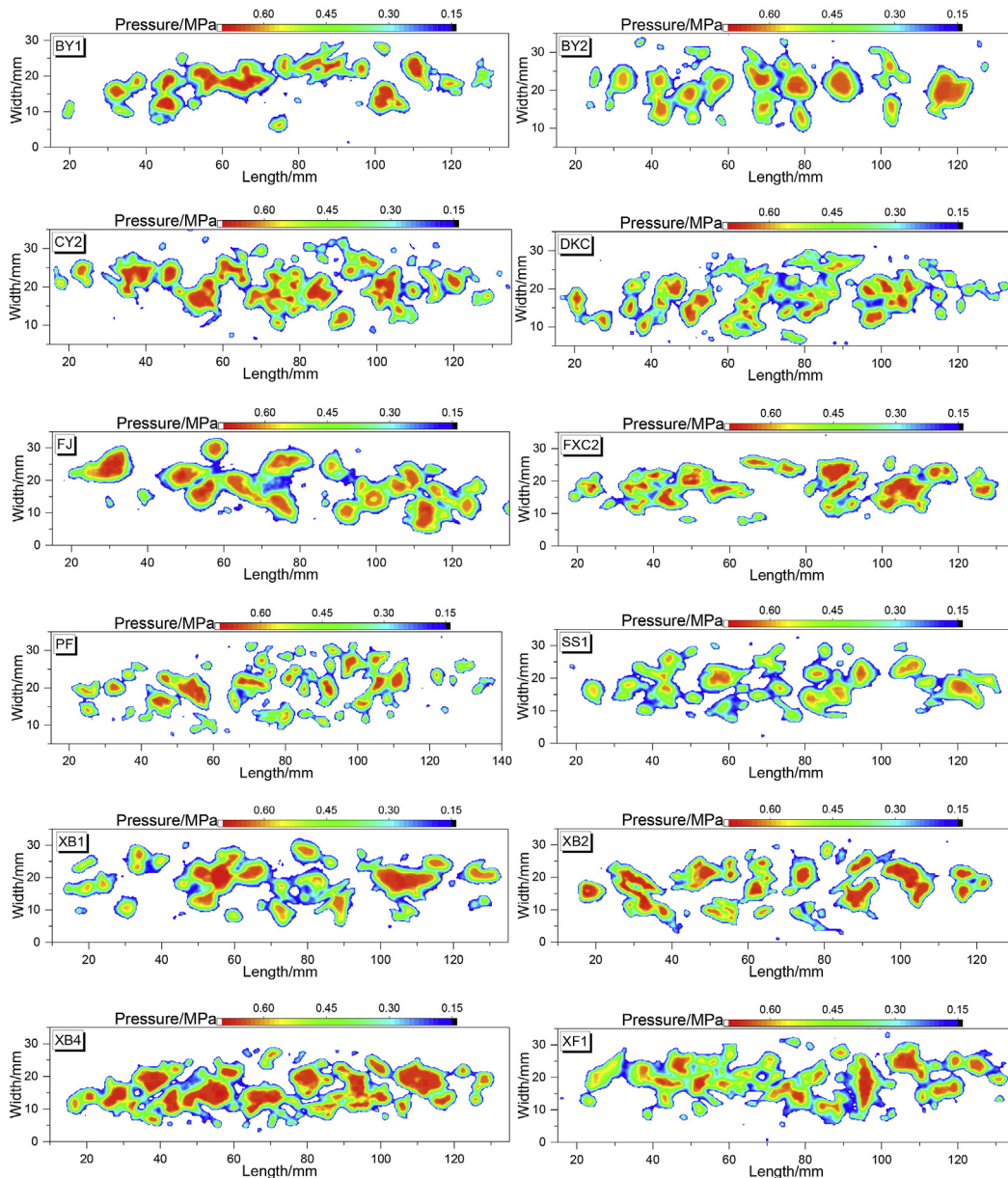
Appendix B. Typical interface recorded on pressure films for each section

Interfaces recorded on the 2LW film.

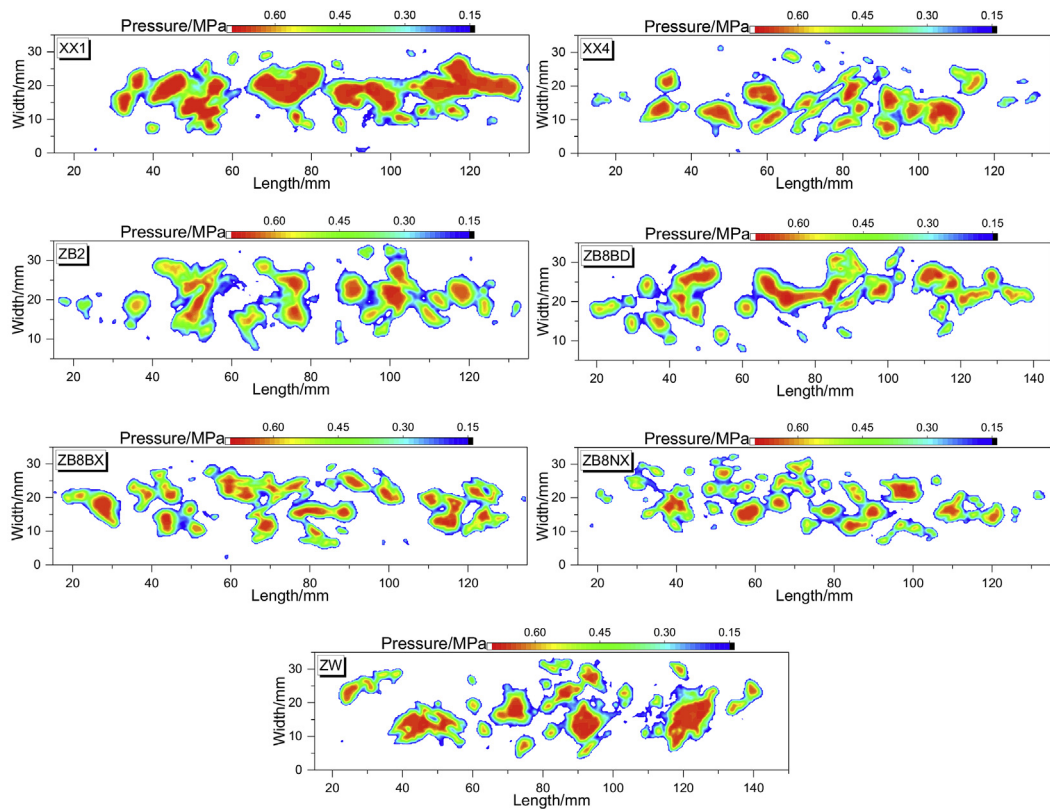




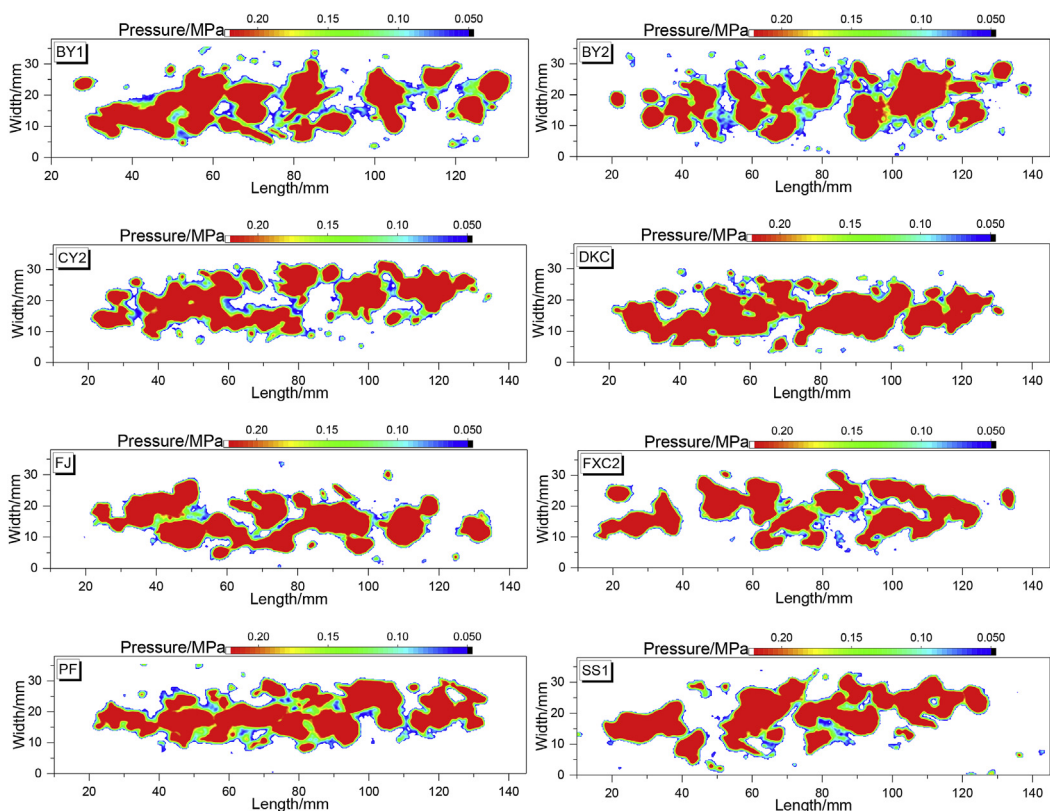
Interfaces recorded on the 3LW film.



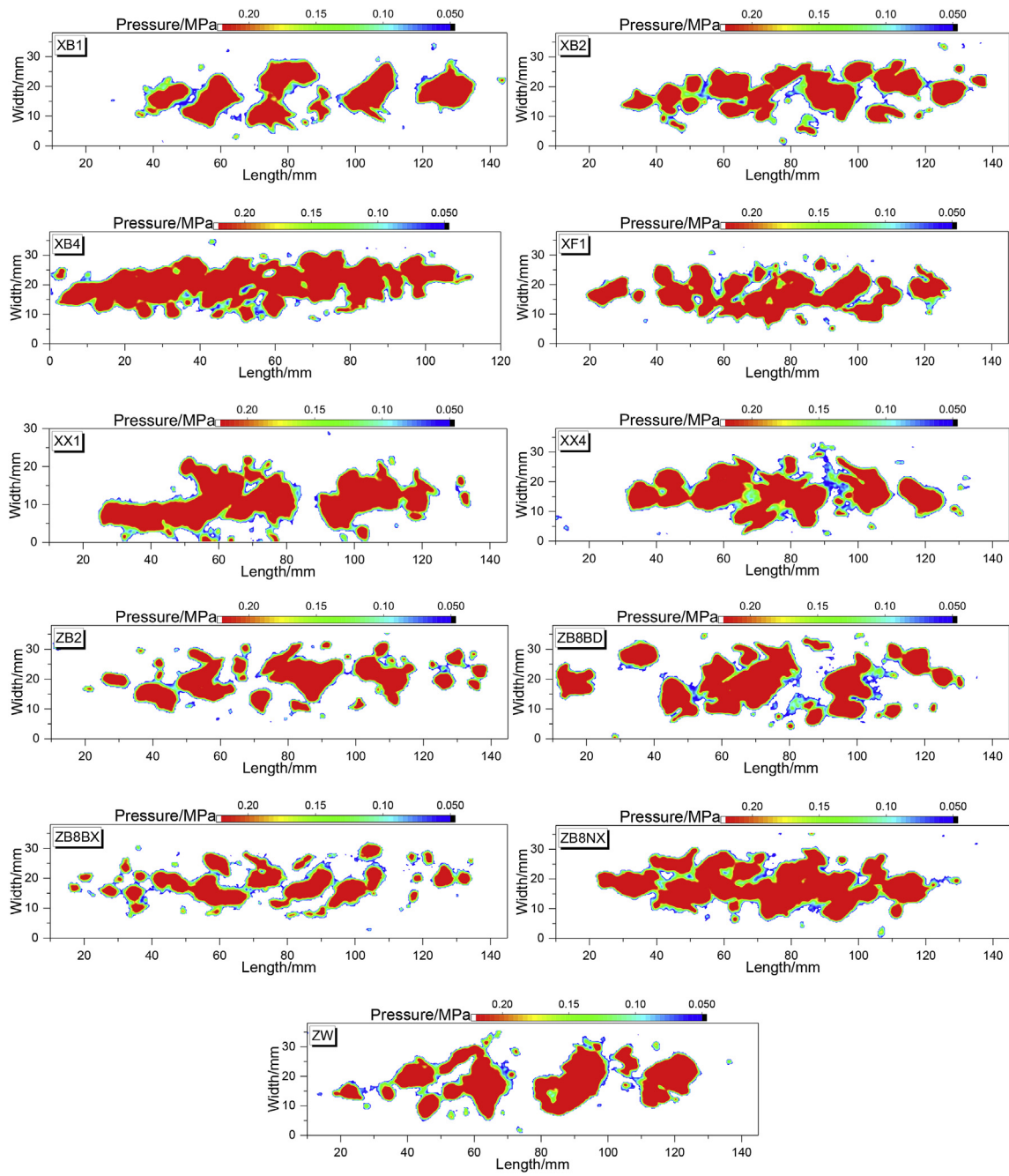
(continued).



Interfaces recorded on the 4LW film.



(continued).



(continued).

References

- Boduch, M., Fincher, W., 2009. Standards of human comfort. https://soa.utexas.edu/sites/default/disk/preliminary/preliminary/1-Boduch_Fincher-Standards_of_Human_Comfort.pdf. (Accessed 12 October 2018).
- Breytenbach, J., Anochie-Boateng, J.K., Paige-Green, P., van Rooy, J.L., 2013. Laser-based assessment of road aggregate particle shape and texture properties with the aim of deriving comparative models. *J. S. Afr. Inst. Civ. Eng.* 55, 30–35.
- Calvey, J.C., Shackleton, J.P., Taylor, M.D., Llewellyn, R., 2015. Engineering condition assessment of cycling infrastructure: cyclists' perceptions of satisfaction and comfort. *Transport. Res. Pol. Pract.* 78, 134–143.
- Cheli, F., Braghin, F., Brusarosco, M., Mancuso, F., Sabbioni, E., 2011. Design and testing of an innovative measurement device for tyre–road contact forces. *Mech. Syst. Signal Process.* 25 (6), 1956–1972.
- Chen, B., Zhang, X., Yu, J., Wang, Y., 2017. Impact of contact stress distribution on skid resistance of asphalt pavements. *Constr. Build. Mater.* 133, 330–339.
- Chou, C.-P., Lee, W.-J., Chen, A.-C., Wang, R.-Z., Tseng, I.C., Lee, C.-C., 2015. Simulation of bicycle-riding smoothness by bicycle motion analysis model. *J. Transport. Eng.* 141 (12), 04015031.
- Creality 3D Technology Co, L., 2017. Customer manual of CR-10 3D printer. <https://www.cxsw3d.com/ziliaoxiazai46.html>.
- Dao, T.-K., Chen, C.-K., 2012. A study of bicycle dynamics via system identification approaches. *J. Chin. Inst. Eng.* 35 (7), 853–868.
- Fujifilm, 2015. Specifications and operational environment of pressure measurement film. <http://www.fujifilm.com/products/prescale/prescalefilm/#specifications>. (Accessed 25 April 2018).
- Gao, J., Sha, A., Huang, Y., Hu, L., Tong, Z., Jiang, W., 2018. Evaluating the cycling comfort on urban roads based on cyclists' perception of vibration. *J. Clean. Prod.* 192, 531–541.
- Griffin, M.J., 1990. 11 - methods for measuring and evaluating whole-body vibration exposures. In: Griffin, M.J. (Ed.), *Handbook of Human Vibration*. Academic Press, London, pp. 453–483.
- Hölzel, C., Höchtl, F., Senner, V., 2012. Cycling comfort on different road surfaces.

- Procedia Engineering 34, 479–484.
- Hu, L., Yun, D., Liu, Z., Du, S., Zhang, Z., Bao, Y., 2016. Effect of three-dimensional macrotexture characteristics on dynamic frictional coefficient of asphalt pavement surface. *Constr. Build. Mater.* 126, 720–729.
- ISO4287, 1997. Surface Roughness - Terminology - Part 1: Surface and its Parameters.
- ISO-2631, 1997. Mechanical Vibration and Shock Evaluation of Human Exposure to Whole-Body Vibration - Part 1 General Requirements. International Organization for Standardization.
- JTG F40-2004, 2004. Technical Specification for Construction of Highway Asphalt Pavement. Inspection and Quarantine of the People's Republic of China, Beijing.
- Li, H., Harvey, J., Thigpen, C., Wu, R., 2013a. Surface Treatment Macrotexture and Bicycle Ride Quality. University of California Pavement Research Center, Davis, CA. Vol. Research Report: UCPRC-RR-2013-07.
- Li, H., Harvey, J., Wu, R., Thigpen, C., Louw, S., Chen, Z., Rezaie, A., 2013b. Preliminary Results: Measurement of Macrotexture on Surface Treatments and Survey of Bicyclist Ride Quality on Mon-198 and SLO-1 Test Sections (Vol. Technical Memorandum: UCPRC-TM-2013-07). University of California Pavement Research Center, Davis, CA.
- Li, T., Burdisso, R., Sandu, C., 2018. Literature review of models on tire-pavement interaction noise. *J. Sound Vib.* 420, 357–445.
- Liang, C., Wang, G., An, D., Ma, Y., 2013. Tread wear and footprint geometrical characters of truck bus radial tires. *Chin. J. Mech. Eng.* 26 (3), 506–511.
- Luo, W., 2018. Autonomous Cars, Shared Bikes Due for Improvement, China daily.
- Nayak, S.R., Mishra, J., Palai, G., 2018. A modified approach to estimate fractal dimension of gray scale images. *Optik* 161, 136–145.
- Ricci, M., 2015. Bike sharing: a review of evidence on impacts and processes of implementation and operation. *Res. Transp. Bus. Manag.* 15, 28–38.
- Rybarczyk, G., Wu, C., 2010. Bicycle facility planning using GIS and multi-criteria decision analysis. *Appl. Geogr.* 30 (2), 282–293.
- Song, Y., Li, Y., Song, W., Yee, K., Lee, K.Y., Tagarielli, V.L., 2017. Measurements of the mechanical response of unidirectional 3D-printed PLA. *Mater. Des.* 123, 154–164.
- Taylor, M.D., Edgar, A., Raine, M., 2017. Cyclist Exposure to Hand-Arm Vibration and Pavement Surface Improvement in the City of Edinburgh. Scottish Transport Applications and Research Conference. Technology and Innovation Centre, University of Strathclyde.
- Taylor, M.D., Edgar, A., Raine, M., 2018. Scottish cycling pavement assessment using hand-arm vibration exposure. *Infrastruct. Asset Manag.* 0 (0), 1–16.
- Torbic, D., El-Gindy, M., Elefteriadou, L., 2003. Methodology for quantifying whole-body vibration experienced by cyclists. *Int. J. Veh. Des.* 31, 452–480.
- Van Put, A., Vertes, A., Wegrzynek, D., Treiger, B., Van Grieken, R., 1994. Quantitative characterization of individual particle surfaces by fractal analysis of scanning electron microscope images. *Fresenius J. Anal. Chem.* 350 (7), 440–447.
- Zhang, K., Zhang, Z., Luo, Y., Huang, S., 2017. Accurate detection and evaluation method for aggregate distribution uniformity of asphalt pavement. *Constr. Build. Mater.* 152, 715–730.
- Zhang, L., Zhang, J., Duan, Z.-y., Bryde, D., 2015. Sustainable bike-sharing systems: characteristics and commonalities across cases in urban China. *J. Clean. Prod.* 97, 124–133.
- Zhang, X., Liu, T., Liu, C., Chen, Z., 2014. Research on skid resistance of asphalt pavement based on three-dimensional laser-scanning technology and pressure-sensitive film. *Constr. Build. Mater.* 69, 49–59.